Astronomy & Astrophysics manuscript no. s106˙fcrao˙0409˙2007
September 4, 2007
© ESO 2007

A multiwavelength study of the S106 region

III. The S106 molecular cloud as part of the Cygnus X cloud complex

N. Schneider[1,4], R. Simon[4], S. Bontemps[2], F. Comerón[3], and F. Motte[1]

[1] DAPNIA/SAp CEA/DSM, Laboratoire AIM CNRS - Université Paris Diderot, F-91191 Gif-sur-Yvette, France
[2] OASU/LAB-UMR5804, CNRS, Université Bordeaux 1, 33270 Floirac, France
[3] ESO, Karl-Schwarzschild Str. 2, 85748 Garching, Germany
[4] I. Physikalisches Institut, Universität zu Köln, Zülpicher Straße 77, 50937 Köln, Germany

September 4, 2007

ABSTRACT

Context. The distance to the wellknown bipolar nebula S106 and its associated molecular cloud is highly uncertain. Values between 0.5 and 2 kpc are given in the literature, favoring a view of S106 as an isolated object at a distance of 600 pc as part of the 'Great Cygnus Rift'. However, there is evidence that S106 is physically associated with the Cygnus X complex at a distance of ∼1.7 kpc (Schneider et al. 2006). In this case, S106 is a more massive and more luminous star forming site previously thought.
Aims. We aim to understand the large-scale distribution of molecular gas in the S106 region, its possible association with other clouds in the Cygnus X south region, and the impact of UV radiation on the gas. This will constrain the distance to S106.
Methods. We employ a part of an extended ^{13}CO and C^{18}O 1→0 survey, performed with the FCRAO, and data from the MSX and Spitzer satellites to study the spatial distribution and correlation of molecular cloud/PDR interfaces in Cygnus X south. The 2MASS survey is used to obtain a stellar density map of the region.
Results. We find evidence that several molecular clouds including S106 are directly shaped by the UV radiation from members of several Cygnus OB clusters, mainly NGC 6913, and are thus located at a distance of ∼1.7 kpc in the Cygnus X complex. The definition of OB associations in terms of spatial extent and stellar content in the Cygnus X south region is revised.

Key words. interstellar medium: clouds – individual objects: S106 – molecules – kinematics and dynamics – Radio lines: ISM

1. Introduction

The H II region S106 in Cygnus is famous for its bipolar emission nebula (e.g., Oasa et al. 2006). The nebula is excited by the O-star S106 IR and embedded in a molecular cloud which was studied in different molecular line tracers at various angular resolutions. Observations using lower-J CO lines at a resolution of ∼1′ (Lucas et al. 1978; Bally & Scoville 1982; Schneider et al. 2002) revealed a cloud with an extent of ∼20′×25′ and two emission peaks, separated by ∼3′, centering S106 IR. The eastern peak has the shape of a 'lane' that is devoid of radio continuum emission, which is interpreted by some authors (Bally & Scoville 1982; Ghosh et al. 2003; Qin et al. 2005) as a massive disk or torus around S106 IR. The western peak is also seen in NH_3 emission (Stutzki et al. 1982). It is more diffuse and has an emission distribution elongated northsouth blocked by the lobes of the H II region. A secondary site of star formation ∼5′ south of S106 IR was detected as a peak in CO emission containing an embedded cluster (Rayner 1994) seen also with 2MASS[1] (Schneider et al. 2002). See also the chapter 'S106' by Hodapp in the 'Handbook of star formation' (Reipurth 2007) for more information on S106.

The majority of the observations, however, concentrated on mapping the dense gas immediately around S106 IR at higher angular resolution in various atomic and molecular tracers (e.g., Churchwell & Bieging 1982; Little et al. 1995; Schneider et al. 2002, 2003) and the continuum (Richer et al. 1993; Vallée et al. 2005; Motte et al. 2007). Optically thick molecular lines revealed strong

Send offprint requests to: N. Schneider
Correspondence to: nschneid@cea.fr

[1] The Two Micron All Sky Survey (2MASS) is a joint project of the University of Massachusetts and the Infrared Processing and Analysis Center/California Institute of Technology, funded by the National Aeronautics and Space Administration and the National Science Foundation.

outflow emission close to S106 IR. This star also powers a bright photon dominated region (PDR) as seen in atomic Far-infrared (FIR) lines ([C II] 158 μm, [C I] 809 and 370 μm, Schneider et al. 2003) and emission lines of Brγ and H_2 1–0 S(1) (Hayashi et al. 1990).

The range of distances given in the literature for the S106 complex is broad. Early estimates using the kinematic information of S106 give values >2 kpc (e.g., Reifenstein et al. 1970; Maucherat 1975). However, S106 is located at Galactic longitude ∼76.5° where the local Galactic arm, the Perseus arm, and the outer Galaxy are found along the same line of sight, covering distances between a few hundred pc and 8 kpc. In this direction, radial velocities of nearby clouds are close to zero and thus do not provide *reliable* distance estimates. Distances derived with other methods (Eiroa 1979; Staude 1982; Rayner 1994) are smaller (500 to 600 pc). These values are commonly used for the S106 region.

In this paper, we study the spatial and kinematic distribution of molecular gas in S106 and place this cloud in the context of other objects in the Cygnus X region. To date, extrinsic influences on S106 (shock-compression, radiation pressure, and winds from external OB-stars) have not been considered or studied because S106 was seen as an isolated object in the quiescent 'Cygnus Rift' at ∼600 pc distance. We investigate whether the UV radiation of the Cygnus OB1 and OB9 associations and their sub-associations, such as NGC 6913 (M29) and Ber87, affect the S106 molecular cloud and other molecular gas in this region. For this, we compare ^{13}CO emission line maps taken with the FCRAO[2] with mid-IR emission data from MSX[3]. Data from 2MASS are used to determine stellar densities of the brightest stars in order to obtain an overview of the distribution of the star clusters that influence the molecular gas. It is important to constrain the distance to S106 since a larger distance implies that the molecular cloud is more massive and the exciting star S106 IR has an earlier spectral type than previously thought and thus powers a more luminous PDR.

Observational details are given in Sect. 2. Large- and small-scale overlays of ^{13}CO onto mid-IR MSX data are shown in Sect. 3, the observed molecular line maps are presented and some cloud properties are determined from the CO data. In the discussion (Sect. 4), we briefly review existing distance estimates for S106, discuss the 'Cygnus Rift', and finally propose a new scenario for S106, which is, in our view, closely associated with the Cygnus X molecular cloud complex at a distance of ∼1.7 kpc (Schneider et al. 2006). Section 5 summarizes the paper.

2. Observations

2.1. FCRAO CO observations

Coverage

We use data from an extensive molecular line survey of the whole Cygnus X region taken with the FCRAO 14m telescope. An area of 35 deg^2 was observed in ^{13}CO and C^{18}O 1→0 using the 32 pixel "Second Quabbin Optical Imaging Array" (SEQUOIA) in an On-the-Fly (OTF) observing mode. The data were obtained between 2003 December and 2006 January and will be presented in more detail in Simon et al. (2007, in prep.). In the current paper, we concentrate on ^{13}CO 1→0 emission from an area of 3×3 deg^2 covering the molecular clouds in the south-western part of the survey (named 'Cygnus X south' in Schneider et al. 2006), and in ^{13}CO and C^{18}O 1→0 emission from a region of 40′×40′ extent, centered on S106.

OTF-mapping

The Cygnus X data were assembled from individual OTF maps (*footprints*) of 20′×10′ size. The integration time was 1 s for each of the 64 simultaneously recorded spectra, 32 in ^{13}CO and 32 in C^{18}O, as the telescope moved continuously across the sky. One OTF footprint map thus took ∼30 minutes including overheads. The maps were observed with some overlap to compensate for the less dense sampling at the edges of the footprint maps and allow for uniform noise in the final, merged data set. Due to the OTF observing mode, the resulting grid of spectra is very dense and highly oversampled. The spectra were gridded on a 22″.5 raster before being merged into the final data set. The FWHM of the FCRAO at the observed frequencies is ∼46″. The spectra have a mean 1σ rms noise level of ∼0.2 K on a T_A^* antenna temperature scale, i.e., not corrected for the main beam efficiency of ∼0.48 at 110 GHz.

Backend

The receiver was used in combination with a dual channel correlator (DCC), configured to a bandwidth of 25 MHz, 1024 channels, and a velocity sampling of 0.066 km s^{-1}. With this correlator, two independent intermediate frequencies (IFs) could be processed for each of the 32 pixels, and therefore, 32 spectra could be observed simultaneously at 110 and 109 GHz (^{13}CO and C^{18}O).

Pointing and Calibration

Pointing and calibration were checked regularly at the start of the Cygnus LST interval and after transit of Cygnus (no observations were performed at elevations higher than 75°). Pointing sources were SiO masers of evolved stars, i.e., χ-Cyg, R-Leo and T-Cep, depending on LST-time. The calibration was checked regularly on the position of peak emission in DR21 and found to be consistent within 10%.

3. Results and analysis

3.1. Large-scale correlation of molecular line and mid-IR emission

Figure 1 shows a part of the ^{13}CO 1→0 FCRAO survey of the Cygnus X region overlaid as contours on a color image of mid-IR emission at 8.3 μm (MSX Band A with an angular resolution of 20″). The CO emission is integrated over a velocity range of –10 to 20 km s^{-1} so that

[2] Five College Radio Astronomy Observatory
[3] Midcourse Space Experiment

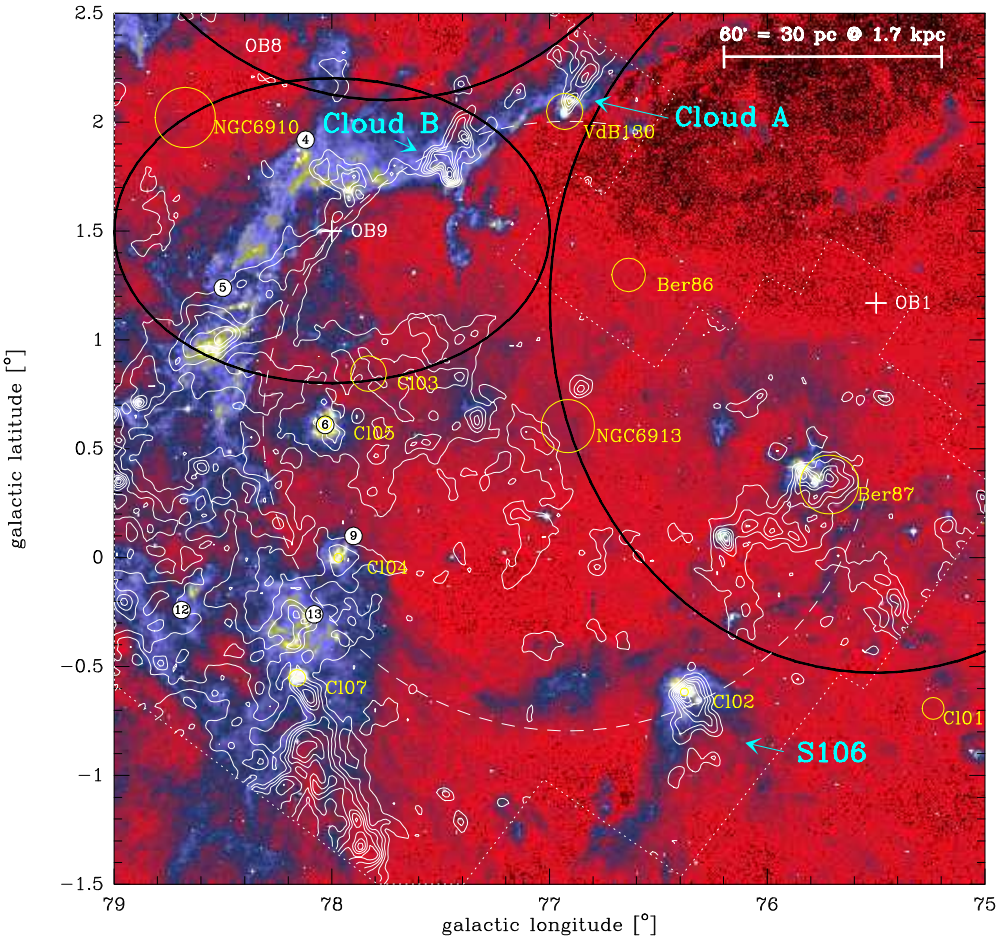

Fig. 1. Overlay of ^{13}CO 1→0 emission in the velocity range –10 to 20 km s^{-1} (white contours) on an 8 μm image of MSX in the Cygnus X south region containing S106. The map shows about 25% of the FCRAO survey area (Simon et al. 2007, in prep.) the boundary of which is indicated by a short-dashed line. Contours are from 4 to 36 km s^{-1} in steps of 4 km s^{-1}, the color scale is (0.05–1.0)×10^{-5} W m^{-2} sr^{-1}. The large black ellipses represent the extent of the OB8, OB9 and OB1 associations and crosses are their center. Yellow, small circles show known clusters, i.e., NGC 6913, NGC 6910, Ber86, Ber87, as well as Cl02–7 (Le Duigou & Knödlseder 2002). Small circles with numbers indicate known H II regions DR4,5,6,9,12, and 13 (Downes & Rinehart 1966). The long-dashed circle encloses a cavity largely devoid of mid-IR emission.

all molecular clouds seen in Cygnus X (Schneider et al. 2006) are included. The molecular cloud associated with S106 is located at l=76.4° and b=–0.7°.

The emission at 8 μm is a tracer of PDR-interfaces because the UV radiation from massive stars heats small grains and polycyclic aromatic hydrocarbons (PAHs) which re-radiate part of their energy at this wavelength. The point-like sources are either (clusters of) young massive and bright stars or embedded red objects that are usually massive protostars. The most prominent feature seen in the MSX image is a large-scale circle (indicated by a long-dashed line in Fig. 1) of bright mid-IR emission approximately centered on NGC 6913. The circle is not closed, but shows a lack of emission towards the cluster Ber86 and the center of Cyg OB1. The star-forming regions within the molecular clouds are found to be arranged on this circle. Some contain identified star clusters (Cl02–5, Cl07 after the nomenclature of Le Duigou & Knödlseder 2002, and Ber87), others show strong mid-IR emission due to embedded clusters (e.g., at l=76.2°, b=0.1°) and/or due to external excitation. The most prominent examples for the latter case are found at l=76.8°, b=2.1° (Cloud A), at l=77.5°, b=1.8° (Cloud B), and S106. They are bright-rimmed, globular-shaped molecular clouds with a tail of emission in mid-IR and CO pointing away from the circle center and are discussed in more detail in the next section.

There are, however, two examples where CO emission and mid-IR emission do not correspond well, i.e., towards an extended, diffuse area south-east and east of NGC 6913, and a region of rather compact clouds south of Cl07. The non-correlation with mid-IR emission does not imply that these clouds are not correlated with the Cygnus X clouds since they can be slightly displaced in the fore- or background with respect to the bulk emission. However, they can also be related to the 'Cygnus Rift'. We will come back to this point in Sect. 4.2.

The large scale distribution of mid-IR/CO emission suggests that the center of excitation for the PDR cloud surfaces is located close to the circle center. Obviously, the open cluster NGC 6913 is the first candidate to be the

exciting source. It is seen as one of the nuclei of OB1 and contains around 100 stars (Wang & Hu 2000) even though only 2 OB-stars were identified (Wang & Hu 2000; Boeche et al. 2004). Other nuclei of OB1 are Ber86 and Ber87 close to NGC 6913. At this point, we only state that a source of UV radiation close to the location of NGC 6913 may have created the observed cavity in mid-IR emission and the circle of PDR emission where the ionization fronts hit the (molecular) gas.

3.2. Small-scale correlation of molecular line and mid-IR emission

Figure 2 shows the prominent PDR interfaces of S106 and two other clouds in detail (Cloud A and B in Figure 1) to illustrate the effect of stellar winds/UV radiation that are shaping the molecular clouds. In addition, we show position-velocity cuts in ^{13}CO to illustrate the velocity structure.

In **Cloud A** (Fig. 2a), two mid-IR point sources are located at the tip (∼2 pc separation, assuming a distance of 1.7 kpc) of the dense molecular cloud. Around these sources, a ring-like structure in mid-IR emission is observed that corresponds to VdB130, a single star or small star cluster in a reflection nebula, similar to 'Cloud B' (see below). The H II region DWB34 listed in the catalog of Dickel et al. (1969) is indicated in the plot. The tail (∼10 pc length) of the cloud is more dispersed in CO and mid-IR emission and cleary points away from the cavity (compare with Fig. 1). The position-velocity cuts (lv-cuts) go along the two main flow directions of the gas. Only a small velocity gradient can be identified for Cut 2. Cut 1, however, shows a strong, clearly defined gradient in velocity (+0.5 km s^{-1}/pc). Similar values are found in much smaller molecular 'globules' (sizes of typically 0.5 pc for the head and 1.5 pc for the tail, see, e.g., White et al. 1997). However, the mechanisms at work that are responsible for the observed large-scale gas flows in Cloud A are most likely the same, i.e., influence of UV-radiation and stellar winds of OB stars.

The structure of mid-IR and ^{13}CO emission around **Cloud B** (Fig. 2b) is very complex and we observe several, overlaying features. The large scale emission in both tracers shows a similar distribution as for Cloud A with a dense clump of molecular gas, facing the UV field, and a more dispersed tail. Embedded in the main CO peak, an MSX point source corresponds to Mol121 (Molinari et al. 1998). This is an ultra-compact H II region which contains a small cluster of stars seen in near-IR by Deharveng et al. (2005). The same authors identified a nearly circular H II region (their source 'X' and marked as such in the plot) that was not listed in the DWB-catalog of optically visible H II regions. The edge of the main CO peak is lit up by UV radiation, as seen in the bright, narrow rim of MSX emission. Extending to the right and left of the CO peak, a bow-shaped feature in CO and mid-IR emission is seen, suggesting that here we also observe compressed, UV illuminated, dense gas. This structure is clearly visible in the lv-cut 2 (between 7′ and ∼10′), covering a velocity range of ∼6 km s^{-1} that is much larger than a typical internal velocity dispersion of a quiescent molecular cloud. Cut 1 goes along one of the main tail axes. The outflow from Mol121 is seen at ∼8′. The CO emission in the tail is complex, suggesting on first sight a second outflow source around 18′. However, a careful analysis of the spectra shows that the large range of velocities observed (–3 to 4 km s^{-1}) is mainly caused by several overlapping cloud components and a high internal velocity dispersion of the gas. The existence of an outflow source can not be ruled out, but requires higher angular resolution molecular line observations.

In Cloud A and B, the mid-IR emission is clearly shifted towards the edge of the clouds and the center of the cavity. This stratified distribution of CO and mid-IR emission together with the globular shape of the clouds is strong evidence that the origin of the exciting UV photons is inside the large-scale circle.

The *lower intensity* mid-IR emission in **S106** forms a bow-shaped feature with two diffuse tails pointing away from the center of the circle in Fig. 1. This shape is clearly caused by external UV radiation from inside the large-scale cavity. The CO emission has a similar distribution but is more concentrated to the inside of the bow-shaped mid-IR emission, suggesting that the molecular cloud is embedded in a larger cocoon of heated gas, visible in mid-IR emission. The *high-intensity* mid-IR emission is the well-known bipolar nebula S106 whose orientation is nearly orthogonal to the low-intensity mid-IR emission. The exciting UV source is the OB-star S106 IR. Though this star creates a bright PDR in its immediate environment, the UV flux decreases rapidly from a few 10^5 G$_\circ$ at the position of S106 IR down to 10^2 G$_\circ$ in 2′ distance (Schneider et al. 2003). Cut 1 and 2 show a velocity gradient that is smaller (∼0.3 km s^{-1}/pc) than for Cloud A. It seems that the gas here is less dynamic than along Cut 1 in Cloud A and in the shock-compressed region of Cloud B. Strongly visible in both cuts is the outflow emission caused by S106 IR.

In the next section, we discuss in more detail the molecular line emission of the prominent source S106.

3.3. Molecular line maps of S106

The results of our molecular line mapping of S106 in the ^{13}CO and C^{18}O 1→0 transitions are shown in Figs. 3 and 4. In Fig. 3, the ^{13}CO map is overlaid on a color image of 4.5 μm emission obtained from the *Spitzer* space telescope archive. Figure 4 shows the line integrated ^{13}CO and C^{18}O 1→0 maps separately.

Significant ^{13}CO emission is found in the velocity range v= –9 to 6 km s^{-1} while the C^{18}O 1→0 emission is restricted to the velocity range v= –4 to 2 km s^{-1}. Both line maps show the characteristic two-lobe emission distribution east and west of S106 IR (indicated as a star

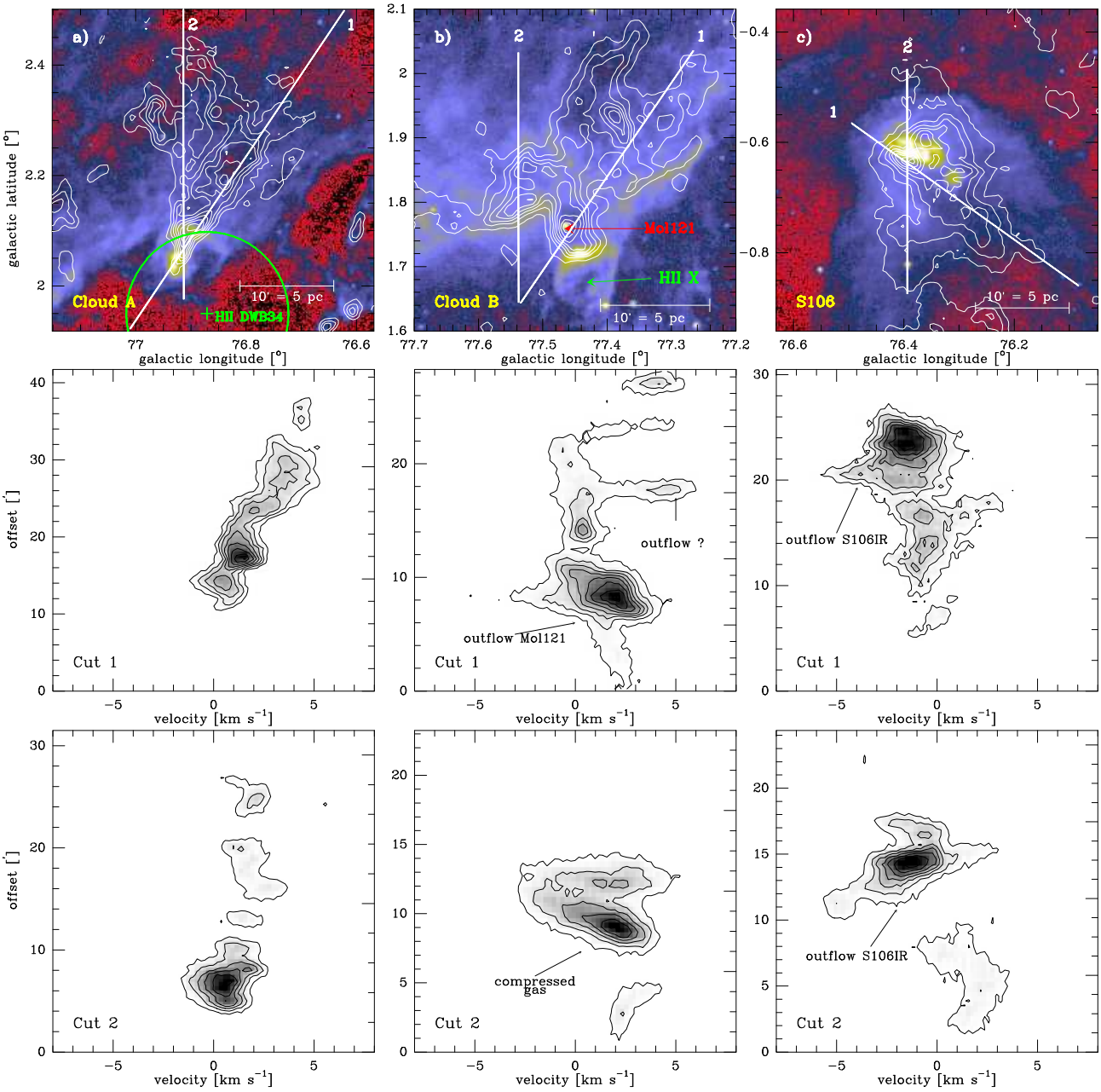

Fig. 2. Top: Cloud A (a), B (b) and S106 (c) in ^{13}CO 1→0 emission (contours) overlaid on mid-IR emission (8 μm from MSX). The bold lines indicate two position-velocity cuts shown in the bottom figures. An offset of 0′ indicates the lower latitude starting point of the cuts. Particular sources are labeled.

in the plot). The lobes of ionized gas from the H II region are nearly orthogonal to the CO emission. This morphology is due to the impact of the radiation and the ionizing wind of S106 IR that created the bipolar lobes which are probably collimated by a very small disk (Persson et al. 1988; Bally et al. 1998). The very turbulent layer between ionized and molecular gas in the lobes becomes visible in Hα images taken with the Hubble Space Telescope (Bally et al. 1998). Beyond these lobes, the cooler molecular gas wraps around the H II region, visible as the bulk emission of the cloud between –3 and 3 km s^{-1}. The strong CO peak southeast of S106 IR is due to outflow emission where the molecular gas is swept up from the cavity walls. It is this part of the S106 molecular cloud that was frequently observed in molecular lines and discussed so we do not go into more detail here. See Schneider et al. (2002) and references therein, as well as a recent publication by Vallée & Fiege (2005).

The ^{13}CO J=1→0 line traces rather low gas densities around $3{\times}10^3$ cm^{-3} and thus gives an overview of the total gas distribution of the S106 molecular cloud. The emission extends more than 20′ to the south, separated into two tails each showing a (weak) peak of emission at its end. The average intensity is a factor ∼3 lower than for the two regions of peak emission close to S106 IR. In contrast, the C^{18}O map shows almost no emission features

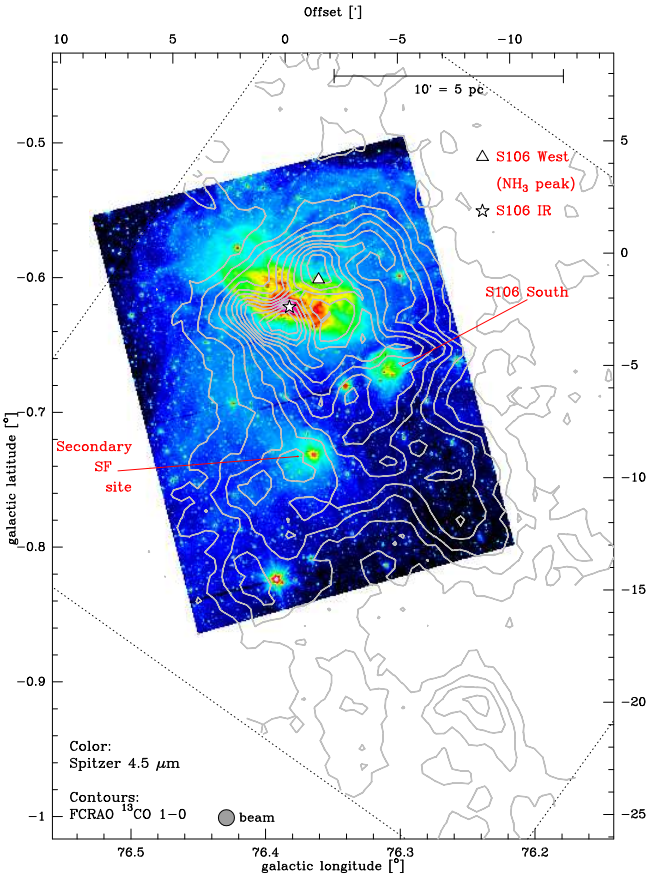

Fig. 3. Line integrated (–9 to 6 km s^{-1}) ^{13}CO 1→0 map overlaid on a color picture of Spitzer 4.5 μm data. CO-contours go from 2 (3σ) to 46 K km s^{-1} in steps of 4 K km s^{-1} and the IR-color range from 0 to 1.6×10^6 MJy/sr. The exiting star S106 IR is marked by a star and a peak of NH_3 emission by a triangle. Several secondary star formation sites are indicated, including S106 south and south-east.

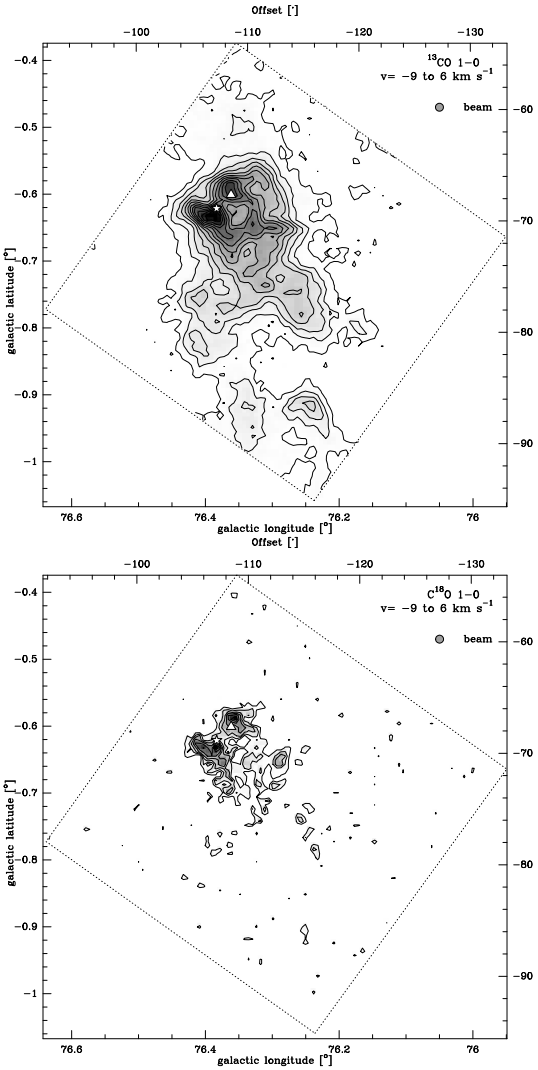

Fig. 4. Maps of the line integrated ^{13}CO 1→0 (top) and C^{18}O 1→0 (bottom) emission in the velocity range v=–9 to 6 km s^{-1} and v=–4 to 2 km s^{-1}, respectively. Contours go from 2 (3σ) to 46 K km s^{-1} in steps of 4 K km s^{-1} for ^{13}CO and 2 (3σ) to 8 K km s^{-1} in steps of 1 K km s^{-1} for C^{18}O.

from the two tails but traces on the more shielded, denser core of molecular gas.

Higher-density tracers such as CS 2→1 and N_2H^+ 1→0 show the same emission distribution (Schneider et al. 2007, in prep.). The ^{13}CO (C^{18}O) 1→0 main beam brightness temperatures vary between a few K (<1 K) in the halo region and the two cloud tails and rise up to ∼15 K (∼4 K) in the bright eastern and western lobes close to S106 IR.

The *Spitzer* 4.5 μm data reveal more clearly than the MSX image (Fig. 2) the secondary star formation sites in S106. The S106 south cluster, first deteced by Rayner (1994) and seen in 2MASS images (Schneider et al. 2002), is still embedded in the bulk emission of ^{13}CO and is located at a peak of C^{18}O emission. At l=76.4°, b=–0.83° and at l=76.35°, b=–0.68° rather strong sources are detected but since we do not observe extended emission around these objects, they may well be foreground stars. In contrast, the source in between shows extended emission and may constitute a small cluster of stars. Conforming to the nomenclature in Schneider et al. (2002), we call this source 'S106 south-eastq'. It is, however, not associated with a prominent peak in CO emission. All objects are too far separated in projected distance to be attributed to the cluster of fainter stars detected by Hodapp & Rayner (1991) which has a 1.7′ radius for the 1σ-level of the stellar density distribution.

3.4. Physical properties of the S106 molecular cloud

We decomposed the ^{13}CO 1→0 map into clumps with a Gaussian density and velocity distribution, using the algorithm *Gaussclumps*. See Stutzki & Güsten (1990) and Kramer et al. (1998) for more details on the program and,

e.g., Schneider & Brooks (2004) and Simon et al. (2001) for its application. The clump masses were then calculated assuming optically thin emission and LTE (local thermodynamic equilibrium) as outlined in Schneider et al. (1998). We assume a distance of 1.7 kpc for our mass calculation (see Sect. 4). The total mass of the cloud is then determined to be the sum of all decomposed clumps (98% of the fitted total intensity, 581 clumps in total) which is 7620 $M_\odot$. The average density within the clumps is then 10^3 cm^{-3}. The mass is consistent with former estimations when scaled up, with a distance of 1.7 kpc. Bally & Scoville (1982) determined 9710 $M_\odot$ based on FCRAO ^{13}CO 1→0 data, and Lucas et al. (1978) estimated a mass of 12000 $M_\odot$ using ^{13}CO 1→0 observations from the MWO 5 m telescope.

A fit to the clump-mass distribution (the number of clumps dN within the mass interval dM, described by the power-law $dN/dM \propto M^{-\alpha}$, see Kramer et al. 1998) gives α=1.62. This is in accordance with values around 1.7 determined from former CO observations at different angular scales (Schneider et al. 2002).

4. Discussion

4.1. Distance estimates for S106

The commonly used distance for S106 is <1 kpc. Early kinematic distances gave much larger values, i.e., 2.3 kpc (Reifenstein et al. 1970; Pipher et al. 1976), and 5.7 kpc (Maucherat 1975). Since local clouds in the direction of S106 have radial velocities close to zero (see Sect. 1), kinematic distances are not reliable. Eiroa et al. (1979) determined a distance of 500 pc with IR-photometry of the exciting star S106 IR. This method, however, requires a source model for S106 IR and does not give a single solution. In their paper, the best fit for the energy spectrum of S106 was obtained with a B0–O8 main sequence star at A_v=21^m. Staude et al. (1982) derived a distance of 600 pc using UBVI photometry of 8 stars which already represents a very low number statistic. They observed a sudden increase by two magnitudes of A_v starting at a distance of 600 pc and attribute that to extinction due to the 'Cygnus Rift', an extended area of gas at that distance. This, however, does not imply that the molecular cloud of S106 is located at the distance of the rift; it could well be further away. Due to these uncertainties, the distances derived by the methods outlined above were long disputed. Neckel (1990, priv. communication) favors a distance of 2 kpc on the basis of a larger number of foreground stars seen on Palomar Observatory Sky Survey Plates. Rayner (1994) determines a distance of at least 1.2 kpc by using J–H versus H–K diagrams, equally based on a large number of star counts.

Another argument to place S106 at a distance of ≤600 pc could be that the H II region is partly visible in the optical and must thus be located in front of or within the 'Cygnus Rift'. However, in the following section, we give arguments against this scenario.

4.2. S106 and the 'Cygnus Rift'

The 'Cygnus Rift' is a large area of obscuration in optical images of the Cygnus X region and is probably part of the 'Gould Belt', an extended (∼700×1000 pc) cloud structure of low-density gas inclined 20° to the Galactic plane (Guillot 2001). An H_α image and extinction map presented in Schneider et al. (2006, their Fig.1) illustrate the large-scale distribution of this feature. The distance to the Cygnus Rift was determined by photometric studies, concluding that the first reddened stars appear at 430 pc (Straizys et al. 1993, North America Nebula at l=84°) and 800 pc (Ikhsanov 1961, IC 1318 b/c at l=78°). Towards S106, Staude et al. (1982) noticed a jump in A_v of around 600 pc. Figure 5 shows the southern part of the H_α image and an extinction map with A_v up to 10^m (the maximum value is A_v=32^m) with contours of IRAS 100 μm emission overlaid on both images. Comparing both plots, it becomes obvious that the overall large-scale extinction is low and varies across the region. The H II region IC 1318 b/c is clearly visible in the optical image though its distance is around 1.5 kpc (see Schneider et al. 2006 and references therein). The visual extinction in this direction is a few magnitudes (<5^m). S106 appears in the optical image even more obscured than IC 1318 b/c. Its extinction averaged over the 2′ 2MASS resolution is 11^m. Both IC 1318 and S106 are located at the edge of the large-scale smooth, yet low level, extinction of the Cygnus Rift.

However, since one has to distinguish between the diffuse extinction due to the rift and the extinction due to dust within the molecular clouds of Cygnus X (associated with the Cyg OB2 association at a distance of 1.7 kpc) or clouds located further away, we overlaid channel maps of ^{12}CO 1→0 emission taken from the CfA CO survey (Dame et al. 1987) on the optical image. The only velocity range matching approximately the region of obscuration is found between 6 and 20 km s^{-1}. This component was already tentatively identified with the rift emission by Schneider et al. (2006) and Piepenbrink & Wendker (1988). Overlays with our FCRAO ^{13}CO 1→0 data did not conclusively reveal the rift, which implies that the column density of the molecular gas in the rift is very low so that the ^{13}CO line emission is weak. This interpretation is supported by the 100 μm emission that is due to cold dust mixed with molecular gas. As can be seen in Fig. 5b, the 100 μm emission traces much more clearly the dense molecular clouds than the diffuse rift emission. That again implies a low column density of the absorbing material in the rift.

To better separate the extinction due to molecular clouds and the rift, we arbitrarily distinguish the two features by a (blue) A_v =5^m contour line. (Though one has to be aware that the rift extinction also covers part of the Cygnus X clouds). This value is justified since the rift extinction is estimated to be not more than a few magnitudes (Dickel & Wendker 1978). However, not all emission within the A_v >5^m contour, including S106, necessarily arises from one coherent cloud complex at the same distance. The situation is much more complex due to possible

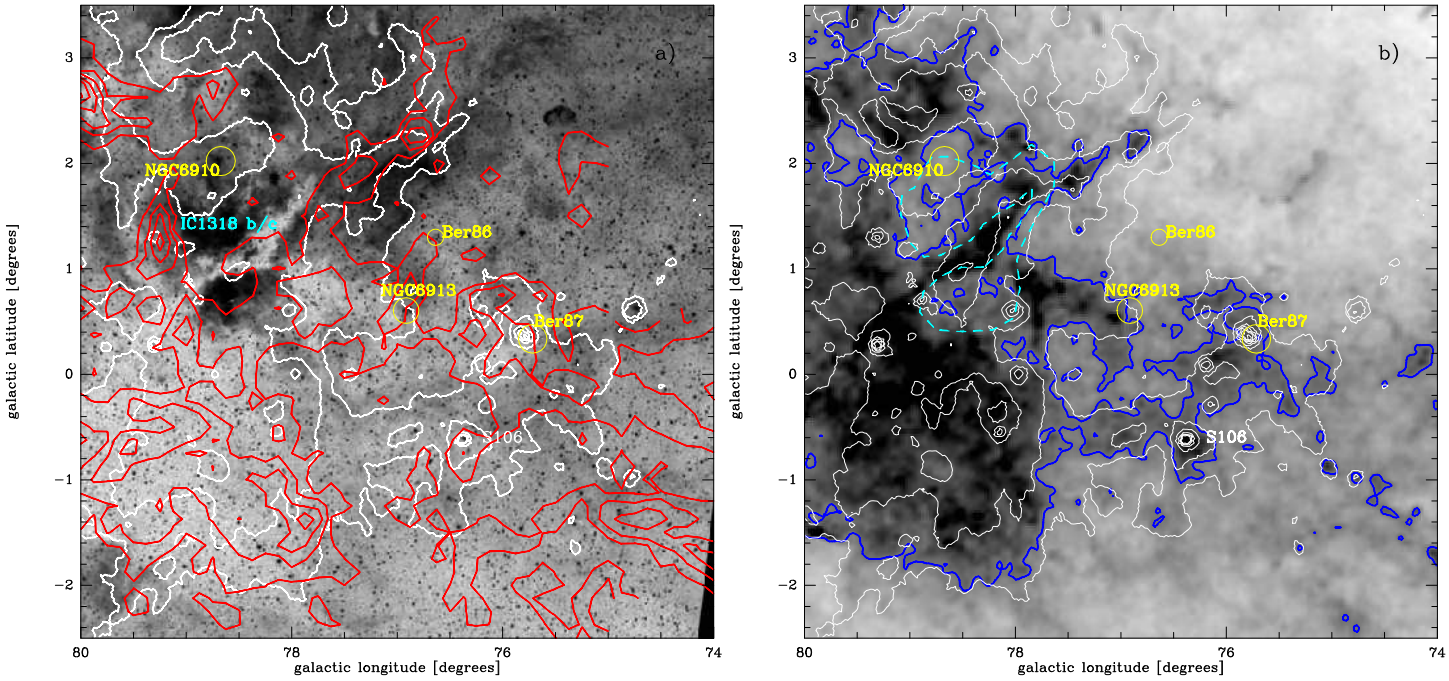

Fig. 5. a) Inverted H_α image (courtesy of William McLaughlin) of the Cygnus X south region. Overlaid are white contours of IRAS 100 μm emission (levels 50,300,500,2000,4000,5000 MJy/sr) and red contours of ^{12}CO 1→0 emission (levels 0.5,1.5,3,5,7,9 K km s^{-1} in the velocity range 6 to 20 km s^{-1}) taken from the Center for Astrophysics CO-survey (Dame et al. 1987). b) Extinction map of the same region in grey scale (A_v=0 to 10^m). This map was obtained from the reddening of J–H and H–K colors using 2MASS data (Bontemps et al., 2007, in prep.). The A_v=5^m contour is outlined in bold blue. Overlaid are the same white contours of IRAS 100 μm emission. The dashed light blue polygon indicates the H II region IC 1318 b/c. Known star clusters are indicated in yellow in both plots.

background features. For example, Boeche et al. (2004) noticed that extinction towards NGC 6913 occults part of the cluster and assigned that to a 'thick interstellar cloud' in the foreground. Figure 5 shows that the obscuration of NGC 6913 is in fact partly due to the *low-density* Cygnus Rift but we also detected significant ^{12}CO and ^{13}CO 1→0 emission (Fig. 1) in that direction and in direction Berkely 87 at velocities between –10 and 6 km s^{-1}. These emission features are not prominent in mid-IR emission, implying that they are possibly background clouds and not associated with Cygnus X.

We suggest now that the high extinction values observed towards S106 are due to its molecular cloud, which is linked to other cloud complexes in the Cygnus X south region through an observed common influence of UV radiation on the clouds. Therefore, S106 is not an isolated object in front of or within the Cgynus Rift, but it is part of the large-scale cloud complexes of the Cygnus X region at the distance of the OB clusters, i.e., larger than 1 kpc.

4.3. S106 as part of the Cygnus X star-forming region

In Sect. 3.1, we presented clear evidence that the UV radiation of the Cygnus OB1 association and its subassociations such as NGC 6913 (M29) and Ber86 affect the S106 molecular cloud and at least two other regions (Cloud A and B). The distance to Cyg OB1 is determined to be 1.25–1.83 kpc (from a compilation of several references in Uyaniker et al. 2001). The distance to NGC 6913 is quoted as between 1.1 and 2.4 kpc (see Boeche et al. 2004 and references therein). The three molecular cloud regions discussed in detail in this paper are part of a ring-like structure (or a 'bubble' if extrapolated to 3D) which is prominent in mid-IR and molecular line emission and shows several active sites of star formation (Clusters Cl2–5 and 7, DR5, 9, and 13). Clouds A and B are linked to the molecular cloud complex of 'Group IV' in the 'Cygnus X south' region (classification from Schneider et al. 2006). It has been noted that this massive (420 000 M$_\odot$), homogeneous complex with emission between –5 and 3 km s^{-1} is influenced by the Cyg OB2 cluster from the eastern side and the Cyg OB1/OB9 associations from the western side (in equatorial coordinates), and that the molecular clouds are located in between. The bulk emission from the S106 molecular cloud is seen in the same velocity range and together with the fact that S106 is shaped by UV radiation and is found on a circle of star-forming sites, we see S106 now as a part of Group IV at the same distance of ∼1.7 kpc. This value, however, remains approximate since all clouds in Cygnus X were given this common distance due to their correlation with Cyg OB2. Moreover, S106 lies on a 'bubble' created by Cyg sub-OB1 association, thus its distance must be within the distance limits of this cluster (1.25–1.83 kpc).

What remains now is to identify more clearly the major source(s) of UV radiation/stellar winds which shape the

molecular clouds on the star-forming circle. For that, we investigate in the following section the properties of the Cyg OB1 cluster and its sub-clusters as well as the general distribution of the Cygnus X OB associations.

4.4. S106 and the Cygnus OB associations

Originally, OB associations were recognized from catalogs of hot stars observed spectroscopically in the optical (Blaauw 1964; Ruprecht et al. 1981; Humphreys 1978). The distances to these stars can be derived (though with large uncertainties) from the calibration of absolute magnitudes with spectral types on the main sequence, In the direction of Cygnus X, 9 OB associations have been defined by Humphreys (1978). These early works are very sensitive to extinction since obscured stars could not be included. The large uncertainties on the individual distances to each star hamper any attempt to get precise distances for groups of stars. In addition, the distance uncertainties make it difficult to recognize coherent groups, especially in crowded regions such as Cygnus.

The distribution of bright 2MASS sources now provides a way to recognize compact (and therefore young) clusters of OB stars. The extinction is less in the near-IR, and from the near-IR colors (J–H and H–K) of the stars, one can roughly estimate the visual extinction toward each star and therefore correct the observed magnitudes to recognize the intrinsically brightest stars. We have derived the stellar density of the brightest K-band sources (magnitude brighter than 10^m) using this extinction correction (see Bontemps et al. 2007, in prep., for details). The resulting contour map overlaid on the MSX image is displayed in Fig. 6. The positions and sizes of the 4 OB associations in the S106 region from the catalog of Uyaniker et al. (2001) are indicated as well. A comparison with the contours of stellar density shows that Cyg OB2 at l=80° is the richest and best defined association and corresponds to the former definition. Towards lower longitudes along the Galactic plane (b∼0.5°), the stellar densities are still high but less consolidated. Within the ellipse characterizing Cyg OB9, a rather compact nucleus can be identified. Towards NGC 6913, two peak regions appear which we name sub1-OB1/9 and sub2-OB1/9. They are *not* identical with the center of the Cyg OB1 and/or OB9 associations but rather form sub-clusters. Inside the Cyg OB1 region, Ber87 shows a detectable cluster of bright stars but in addition, several higher stellar density regions are found.

Mel'nik & Efremov (1995) proposed that OB1, OB8, and OB9 could actually be a single association centered at l=76.8°, b=1.4° at a distance of 1.4 kpc. Inside these associations, several nuclei have been recognized: Ber 87, NGC 6913, and IC4996 for Cyg OB1, and NGC 6910 for Cyg OB9. Altogether, however, only a few tens of optical hot stars are known (119 stars in OB1-8-9 in Mel'nik & Efremov 1995).

The full scenario is probably more complicated and will be discussed in more detail in an upcoming paper (Bontemps et al. 2007, in prep.). However, it becomes obvious that the definition/classification of OB associations in the Cygnus X region needs to be revised. In any case, we can identify sub1-OB1/9 and sub2-OB1/9 (NGC 6913) as the main center of UV radiation for Cloud A, B, and S106. The common effect of both sub-clusters is most likely creatind the cavity in mid-IR emission. It is clearly visible that the highest levels of stellar density fill up the bubble devoid of molecular gas. The circle of compressed gas as we see it in CO and mid-IR emission (Fig. 1) marks the maximum extent of the ionization front created by the sub-clusters. If we consider an expanding ionization front with a velocity of 10 km s^{-1} and assume a radius of 30 pc (approximately what we see around NGC 6913), the age of the cluster must be $3{\times}10^6$ yr. In the literature, we find values between $0.3{-}1.75{\times}10^6$ yr and $10{\times}10^6$ yr (see Boeche et al. 2004 and references therein). An older age would fit in the scenario that NGC 6913 is not very compact but already dispersed.

4.5. The central star S106 IR

The existence of a bright, highly reddened point source near the center of the S106 dark lane, identified as the ionizing source and generally referred to as S106 IR, has been known since the first infrared studies of the region (Sibille et al. 1975; Allen & Penston 1975). Based on visible near-IR and broad-band photometry, Eiroa et al. (1979) derived for S106 IR an approximate distance of 600 pc and a spectral type between B0 and O8. This distance has been adopted in most subsequent studies, but it is important to keep in mind that it was indirectly derived using stellar data, and ionization fluxes, based on estimates which have been superseded by further observations and models. The same applies to the estimate by Staude et al. (1982) which relies on the detection of a relatively small ($A_V \sim 2.5^m$) extinction jump at d∼ 600 pc (most probably the well known Cygnus rift) which does not prove that the S106 cloud is associated with it.

It thus seems timely to reassess the determination of the distance to the ionizing star responsible for the ionization of S106 using the results from state-of-the-art models. We use the infrared photometry in the 2MASS catalog, which is largely free from the uncertainties due to resolution and aperture corrections in the early literature based on single-element observations. The 2MASS colors of S106 IR, $(J-H) = 1.54$, $(H-K_S) = 1.08$, are normal for an early stellar photosphere significantly reddened by foreground extinction. Using the extinction law of Rieke & Lebofsky (1985) and the intrinsic infrared colors of mid- to late-O type stars, we derive $A_K{=}1.86^m$, approximately corresponding to $A_V{=}16.6^m$.

Visible spectroscopy of the nebula, which can be used to constrain the temperature of S106 IR, has been presented by Solf (1980) and Staude et al. (1982). These

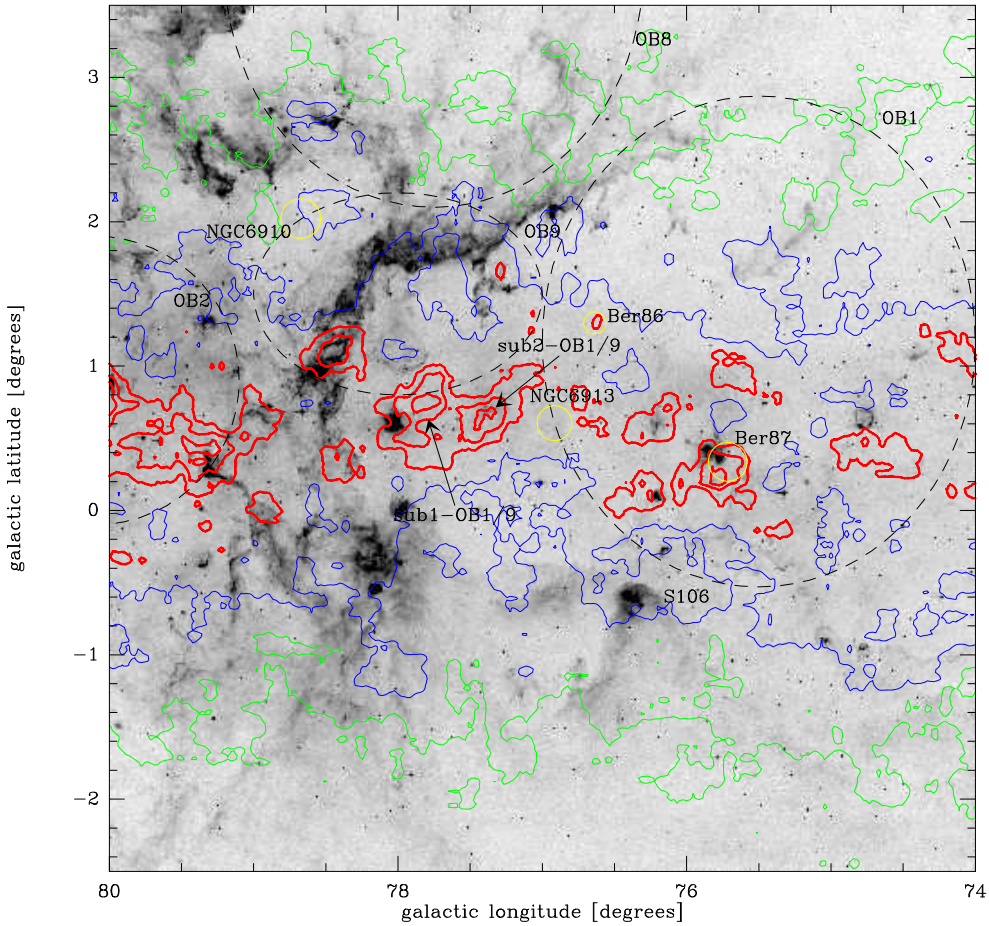

Fig. 6. Contours of stellar densities for stars brighter than A_K=10^m overlaid on a grey scale plot of mid-IR emission taken with MSX. Red, bold contours are 1.1,1.2,1.3, the green contour is 0.9, and the blue contour 0.7. The extent of the Cyg OB 1,2,8 and 9 associations are marked as dashed ellipses and known stellar clusters are indicated in the plot.

latter authors measured the [S II] λ6731 / [S II] λ6717 ratio indicative of a high density ($\sim 10^4$ cm^{-3}) consistent with the compactness of the nebula, whereas the [O III] λ5007 / Hβ ratio corresponds to a temperature in the range $34,000$ K $< T < 36,000$ K according to the single ionizing star models of Stasińska & Schaerer (1997) based on the CoStar stellar atmosphere models of Schaerer et al. (1996). The spectral types yielded by those models are in general between one and two spectral subtypes later than those obtained with more recent atmosphere modeling (Martins et al. 2005). Based on the latter, the temperature interval given above roughly translates into a spectral type O8.5-O7.

Independent support for a temperature near the upper end of the estimated range has been reported by van den Ancker et al. (2000) based on mid-infrared spectroscopy obtained by ISO, from which these authors derive a temperature of 37, 000 K, corresponding to a spectral type O7 in the Martins et al. (2005) calibration. On the other hand, the main-sequence absolute magnitudes M_V given by Martins et al. are relying on an empirical calibration based on emerged O stars, which produces brighter magnitudes than the zero-age main sequence (ZAMS) CoStar models. We have thus used the CoStar temperature-absolute magnitude relationship as being more adequate for an object suspected to be very near the ZAMS such as S106 IR. In this way, we estimate $-3.4 > M_V > -3.8$ for S106 IR, or $-2.57 > M_K > -2.90$ using the intrinsic $(V-K)$ colors of O stars from Martins & Plez (2006). Used in combination with $K_S = 9.49$ measured by 2MASS and the estimated extinction listed above, we obtain a distance modulus $10.20 < DM < 10.53$, with a preference of the upper limit based on the ISO spectroscopy. The corresponding distance lies between 1.1 kpc and 1.3 kpc, somewhat below our proposed distance of 1.7 kpc ($DM = 11.15$) for the S106 region but clearly above the 600 pc ($DM = 8.9$) proposed in earlier studies.

An earlier spectral type for S106 IR implies that more UV photons are produced, creating a more intense UV field which is responsible for the illumination of a bright PDR. Supposing S106 IR is an O8 star, a UV field of $1.5{\times}10^6$ G$_\circ$ at a distance of $5'' = 0.04$ pc or $1.3{\times}10^5$ G$_\circ$ at a distance of $17'' = 0.13$ pc is generated. These values are consistent with the results for the UV field close to S106 IR obtained from observations of FIR-PDR lines (Schneider et al. 2003). One can also directly estimate the ionising flux of S106 IR from the total radio flux of the H II region. We took the flux at 4.8 GHz from Wendker et

al. (1991), of 13.02 Jy which corresponds, for $d = 1.7$ kpc, to an emission measure EM_V of $1.29{\times}10^{61}\,cm^{-3}$ in the optically thin case. Using the typical recombination rate of $2.7{\times}10^{-13}\,cm^3/s$ (Spitzer 1978), this EM_V requires a Lyman flux of $3.5{\times}10^{48}\,s^{-1}$. On the ZAMS, this ionising flux corresponds to an O7 star (Meynet et al. 1994) which is fully consistent with the above estimates of the spectral type of S106 IR.

Though we are confident in our new distance estimate for S106, the ultimate answer could be given by VLBI parallax measurements of the H_2O maser in S106 FIR. Furuya et al. (1999) observed this maser using VLBA during 4 monthly periods which can already serve as a starting point. The future ESA astrometric space mission GAIA will also give the parallax of a large number of at least the OB stars of the region.

5. Summary

By comparing the emission distribution of the ^{13}CO 1→0 line, observed with the FCRAO, with a mid-IR image (8 μm), taken with MSX, in the Cygnus X south region, we reveal the large-scale distribution of molecular gas and how it is influenced by UV radiation. Our prime target was the well-known bipolar nebula S106, which so far in the literature is widely considered as being part of the 'Great Cygnus Rift' at a distance of around 600 pc.

In this paper, we show that several star-forming regions, including S106 and our Clouds A and B, are arranged on a large-scale circle of diameter ∼80 pc seen in both radio and mid-IR wave lengths. From their globular shape and the stratified distribution of 8 μm and CO molecular line emission we conclude that the S106 molecular cloud in the south and two other star-forming regions in the north of the circle are directly shaped by UV radiation from inside the cavity.

The cavity was probably created by radiation and/or stellar wind compression from the massive stars of the OB (sub)-clusters in the Cygnus X region. To identify the main sources for UV radiation, we used the 2MASS survey to obtain a stellar density map of Cygnus X south with stars brighter than magnitude 10 in K-band. We identify the OB (sub)-clusters Cyg OB1,9, and NGC 6913 as the main sources for UV radiation. The distribution of these bright and massive stars shows that the definition of OB associations in terms of spatial extent and stellar content in the Cygnus X south region needs to be revised.

The two clouds on the northern edge of the cavity are part of the 'Cygnus X south' cloud complex (Schneider et al. 2006), which is clearly influenced by members of the Cyg OB1 and OB2 associations. From the large-scale morphology and the fact that the clouds in 'Cygnus X south', Clouds A and B, and S106 are also tightly associated kinematically, we conclude that S106 and Clouds A and B are associated with the large molecular cloud complex forming the 'Cygnus X south region' and have to be within the distance limits of the OB1/2 clusters, i.e., around 1.7 kpc.

Due to this revised larger distance, the S106 molecular cloud is more massive (∼7600 $M_\odot$) than previously thought. The spectral type of the exciting star (S106 IR) must be earlier than O9, which is indicated independently by a high [O III]/H_β ratio in the visible spectrum of S106 IR (Solf 1980).

Acknowledgements. This research made use of data products from the Midcourse Space Experiment. Processing of the data was funded by the Ballistic Missile Defense Organization with additional support from NASA Office of Space Science. This research has also made use of the NASA/ IPAC Infrared Science Archive, which is operated by the Jet Propulsion Laboratory, California Institute of Technology, under contract with the National Aeronautics and Space Administration.

References

Allen, D.A., & Penston, M.V., 1975, MNRAS, 172, 245.
Bally, J., & Scoville, N. Z., 1982, ApJ, 255, 497
Bally, J., Yu, K.C., Rayner, J., Zinnecker, H., 1998, AJ, 116, 1868
Blaauw, A., 1964, ARA&A 2, 213
Boeche, C., Munari, U., Tomaselle, L., Barbon, R., 2004, A&A, 415, 145
Churchwell, E., & Bieging, J. H., 1982, ApJ, 258, 515
Dame, T.M., Ungerechts, H., & Cohen, R.S., et al., 1987, ApJ, 322, 706
Deharveng, L., Zavagno, A., & Caplan, J., 2005, A&A, 433, 565
Dickel, H.R., Wendker, H.J., & Bierritz, J.H., 1969, A&A, 1, 270
Dickel, H.R., & Wendker, H.J., 1978, A&A, 66, 289
Downes, D., & Rinehart, R., 1966, ApJ, 144, 937
Eiroa, C., Elsässer, H., & Lahulla, J. F. 1979, A&A, 74, 89
Furuya, R.S., Kitamura, Y., Saito, M., et al., 1999, ApJ, 525, 821
Ghosh, S.K., Kulkarni, V.K., Ojha, D.K., Verma, R.P., 2003, Bulletin of the Astronomical Society of India, 31, 391
Guillot, P., 2001, in 'From Darkness to Ligth', Edts. T. Montmerle & P. André, ASP Conf. Ser., 243, p.677
Hayashi, S., Hasegawa, T., & Tanaka, M., 1990, ApJ, 354, 242
Hodapp,K.-W., & Rayner, J., 1991, AJ, 102, 1108
Humphreys, R.M., 1978, ApJS, 38, 309
Ikhsanov, R.N., 1961, Soviet Astronomy, Vol. 4, Number 6
Kramer, C., Stutzki, J., Röhrig, R., Corneliussen, U., 1998, A&A, 329, 249
LeDuigou, J.-M., & Knödlseder, J., 2002, A&A, 392, 869
Little, L., Kelly, M., Habing, R., Millar, T., 1995, MNRAS, 277, 307
Lucas, R., Le Squéren, A., Kazès, I., Encrenaz, P. J., 1978, A&A, 66, 155
Martins, F., Schaerer, D., & Hillier, D.J., 2005, A&A, 436, 1049.
Martins, F., & Plez, B., 2006, A&A, 457, 637.
Mel'Nik, A.M., & Efremov, Yu.N., 1995, Astronomy Letters, Vol. 21, Issue 1, p.10
Maucherat, A.J., 1975, A&A, 45, 93
Meynet, G., Maeder, A., Schaller, G., et al., 1994, A&AS, 103, 97
Molinari, S., Brand, J., Cesarone, R., et al., 1998, A&A 336, 339

Motte, F., Bontemps, S., Schilke P., Schneider, N., Menten, K., 2007, accepted by A&A
Oasa, Y., Tamura, M., Nakajima, Y., et al., 2006, AJ 131, 16080
Persson, S. E., McGregor, P. J., & Campbell, B. 1988, ApJ, 326, 339
Piepenbrink, A., & Wendker, H.J., 1988, A&A, 191, 313
Pipher, J.L., Sharpless, S., Kerridge, S.J. et al., 1976, A&A, 51, 255
Qin, S., Wang, J., Zhao, G., Miller, M., 2005, Chin. J. Astron. Astrophys., Vol. 5, No.1 ,1
Rayner, J., 1994, Infrared Astronomy with Arrays, Kluwer Academic Press, p. 185-186
Reipurth, B., 2007, Handbook of low mass star forming regions, ASP
Reifenstein, E. C., Wilson, T. L., & Burke, B.F., 1970, A&A, 4, 357
Richer, J., Padman, R., Ward-Thompson, D., Hills, R.E., & Harris, A.I., 1993, MNRAS 262, 839
Rieke, G.H., & Lebofsky, M.J., 1985, ApJ, 288, 618.
Ruprecht, J., Balazs, B.A., & White, R.E., 1981, Budapest: Akademiai Kiado,
Schaerer, D., de Koter, A., Schmutz, W., Maeder, A., 1996, A&A, 310, 837.
Schneider, N., Stutzki, J., Winnewisser, G., et al., 1998, A&A, 335, 1049
Schneider, N., Simon, R., Kramer, C., Stutzki, J., Bontemps, S., 2002, A&A, 384, 225
Schneider, N., Simon, R., Kramer, C., Kraemer, K., Stutzki, J., Mookerjea, B., 2003, A&A, 406, 915
Schneider, N., & Brooks, K.J., 2004, PASA, 21, 290
Schneider, N., Bontemps, S., Simon, R., Jakob, H., Motte, F., Miller, M., Kramer, C., Stutzki, J., 2006, A&A, 458, 855
Sibille, F., Bergeat, J., Lunel, M., Kander, R., 1975, A&A, 40, 441.
Simon, R., Jackson, J. M., Clemens, D. M., Bania, T. M., & Heyer, M.H. 2001, ApJ, 551, 747
Solf, J., 1980, A&A, 92, 51
Spitzer, L., 1978, Physical processes is the ISM, New-York Wiley Interscience
Stasinńska, G., & Schaerer, D., 1997, A&A, 322, 615.
Staude, H.J., Lenzen, R., Dyck, H.M., et al., 1982, ApJ, 255, 95
Straizys, V., Kazlauskas, A., & Vansevicius, V. et al., 1993, Baltic Astronomy, vol. 2, p. 171
Stutzki, J., Ungerechts, H., & Winnewisser G., 1982, A&A, 111, 201
Stutzki, J., & Güsten, R. 1990, ApJ, 356, L63
Uyaniker, B., Fürst, E., Reich, W., Aschenbach, B., Wielebinski, R., 2001, A&A, 371, 675
Vallée, J.P., Fiege, J.D., & Jason, D., 2005, ApJ, 627, 263
van den Ancker, M.E., Tielens, A.G.G.M., & Wesselius, P.R., 2000, A&A, 358, 1035.
Wang, J.-J., & Hu, J.-Y. 2000, A&A, 356, 118
Wendker, H.J., Higgs, L.A., Landecker, T.L.,1991, A&A, 251, 441
White, G.J., Lefloch, B., Fridlund, C.V.M., et al., 1997, A&A, 323, 931